ISSN 1674-1056
http://cpb.iphy.ac.cn
http://iopscience.iop.org/cpb
中国物理 B
Chinese Physics
中国物理
Chinese Physics B

Superconducting quantum bits

Wei-Yang Liu(刘伟洋), Dong-Ning Zheng(郑东宁), Shi-Ping Zhao(赵士平)
Citation: Chin. Phys. B . 2018, 27(2): 027401. **doi:** 10.1088/1674-1056/27/2/027401

Journal homepage: http://cpb.iphy.ac.cn; http://iopscience.iop.org/cpb

What follows is a list of articles you may be interested in

Bridge-free fabrication process for Al/AlO$_x$/Al Josephson junctions

Ke Zhang(张珂), Meng-Meng Li(李蒙蒙), Qiang Liu(刘强), Hai-Feng Yu(于海峰), Yang Yu(于扬)
Chin. Phys. B . 2017, 26(7): 078501. **doi:** 10.1088/1674-1056/26/7/078501

Validation of the Wiedemann-Franz law in a granular s-wave superconductor in the nanometer scale

A Yousefvand, H Salehi, M Zargar Shoushtari
Chin. Phys. B . 2017, 26(3): 037401. **doi:** 10.1088/1674-1056/26/3/037401

Novel 0-π transitions in Josephson junctions between noncentrosymmetric superconductors

Jun-Feng Liu(刘军丰), Huan Zhang(张欢), Jun Wang(汪军)
Chin. Phys. B . 2016, 25(9): 097403. **doi:** 10.1088/1674-1056/25/9/097403

Retrieval of original signals for superconducting quantum interference device operating in flux locked mode

Liu Dang-Ting, Tian Ye, Zhao Shi-Ping, Ren Yu-Feng, Chen Geng-Hua
Chin. Phys. B . 2015, 24(4): 047402. **doi:** 10.1088/1674-1056/24/4/047402

Switching effects in superconductor/ferromagnet/superconductor graphene junctions

Li Xiao-Wei, Liu Dan, Bao Yan-Hui
Chin. Phys. B . 2013, 22(12): 127401. **doi:** 10.1088/1674-1056/22/12/127401

TOPICAL REVIEW — Slid-state quantum information processing

Superconducting quantum bits*

Wei-Yang Liu(刘伟洋)[1,2], Dong-Ning Zheng(郑东宁)[1,2] and Shi-Ping Zhao(赵士平)[1,2,†]

[1] Beijing National Laboratory for Condensed Matter Physics, Institute of Physics, Chinese Academy of Sciences, Beijing 100190, China
[2] School of Physical Sciences, University of Chinese Academy of Sciences, Beijing 100049, China

(Received 18 September 2017; revised manuscript received 16 October 2017; published online 5 January 2018)

Superconducting quantum bits (qubits) and circuits are the leading candidate for the implementation of solid-state quantum computation. They have also been widely used in a variety of studies of quantum physics, atomic physics, quantum optics, and quantum simulation. In this article, we will present an overview of the basic principles of the superconducting qubits, including the phase, flux, charge, and transmon (Xmon) qubits, and the progress achieved so far concerning the improvements of the device design and quantum coherence property. Experimental studies in various research fields using the superconducting qubits and circuits will be briefly reviewed.

Keywords: superconducting qubit, superconducting quantum computing, quantum physics, quantum optics, quantum simulation

PACS: 74.50.+r, 85.25.Cp, 03.67.Lx, 42.50.–p **DOI:** 10.1088/1674-1056/27/2/027401

1. Introduction

Quantum phenomena in Josephson junctions and superconducting quantum interference devices (SQUIDs), such as macroscopic quantum tunneling, energy level quantization, resonant tunneling, photon-induced transition, and population inversion, have been actively investigated since the 1980s.[1,2] In 1999, the NEC group successfully observed the quantum coherent oscillation of a charge-type superconducting quantum bit (qubit) in the time domain with a period of roughly 100 ps for about 2 ns.[3] Quantum coherence was soon demonstrated also in other types of devices such as the phase qubit,[4,5] the flux qubit,[6] and certain hybridizations like the quantronium qubit.[7]

Quantum coherence is a fundamental property of the superconducting circuits and qubits, which provides the basis for a number of quantum physics studies and the ultimate implementation of quantum computing. Over the past years, quantum coherence times have been improved steadily, roughly by an order of magnitude every three years, to the present time scale of 10 μs–100 μs and beyond. In addition to this, studies of the coupled qubit systems are also progressing. Quantum coherence and entanglements have been demonstrated in coupled systems of around ten qubits or more. Systems with the coupled qubit number up to a thousand or two have been built for implementing the quantum annealing algorithm. These achievements have enabled many interesting studies in quantum physics, atomic physics, quantum optics, quantum simulation, and quantum computation, using the superconducting circuits and qubits as an effective platform.

Extensive and comprehensive reviews in this rapidly advancing field can be found in Refs. [8]–[14]. Here we will briefly review the basic principles behind different types of superconducting qubits, their recent developments, and the ongoing research works in various aspects.

2. Superconducting circuits and qubits

Superconducting circuits, like the usual electrical circuits, contain capacitors, inductors, and (effective) resistors, and have the Josephson junctions and resonators as their key elements. Their fabrications also employ many similar processes in the semiconductor planar technology. In contrast to the usual electrical circuits, the superconducting circuits, which work at milli-Kelvin temperatures, behave quantum mechanically on a macroscopic scale due to the macroscopic nature of the condensed superconducting Cooper pairs and an energy gap separating the dissipative quasiparticles from the condensate.

The central part of the superconducting qubits is the Josephson junction which obeys the Josephson equations:

$$I = I_c \sin\varphi, \quad \dot{\varphi} = 2eV/\hbar, \tag{1}$$

where I_c, φ, and V are the junction's critical current, phase difference across the two electrodes, and the voltage drop, respectively. $\hbar$ is the Planck's constant. When the qubit is built up with a superconducting loop containing Josephson junctions, the following flux quantization condition holds:

$$\varphi = 2\pi(l - \Phi/\Phi_0), \tag{2}$$

in which l is an integer and Φ_0 is the flux quantum. Φ is the total flux enclosed in the loop.

*Project supported by the National Natural Science Foundation of China (Grant Nos. 91321208 and 11674380) and the National Key Basic Research Program of the Ministry of Science and Technology of China (Grant Nos. 2014CB921202, 2015CB921104, and 2016YFA0300601).

†Corresponding author. E-mail: spzhao@iphy.ac.cn

© 2018 Chinese Physical Society and IOP Publishing Ltd

2.1. Phase qubits

The phase qubit features a single Josephson junction biased with a current I, as shown in Fig. 1(a). From the resistively and capacitively shunted junction (RCSJ) model[15] and considering Eq. (1), it is easy to find that the system is governed by

$$m\ddot{\varphi} + (m/RC)\dot{\varphi} = -\partial U(\varphi)/\partial\varphi, \tag{3}$$

$$U(\varphi) = -E_J(\varphi I/I_c + \cos\varphi). \tag{4}$$

Here C and R are junction's capacitance and effective resistance, and $m = (\Phi_0/2\pi)^2 C$, $E_J = \Phi_0 I_c/2\pi$. Equation (3) describes a fictitious particle with mass m moving in a potential $U(\varphi)$ with damping coefficient m/RC. The Hamiltonian of the system can be written as $H = Q^2/2C + U(\varphi)$ with charge $Q = 2en$. The Cooper pair number operator $n = -i\partial_\varphi$ is the quantum-mechanical conjugate to φ.[15]

The qubit has a washboard-like potential $U(\varphi)$, which is depicted in Fig. 1(b) together with the energy levels in a selected well. Experimentally one can tilt the potential by changing I so that the barrier height and the level spacing can be tuned. The bottom two states are used for the qubit states, which can be initialized when the barrier is set sufficiently high and manipulated with microwave pulses. The state readout is accomplished by setting appropriate barrier heights at which tunneling out of the potential well from the ground and excited states can be distinguished. Tunneling results in the switching of the junction from the zero to finite voltage state which is then detected.[5]

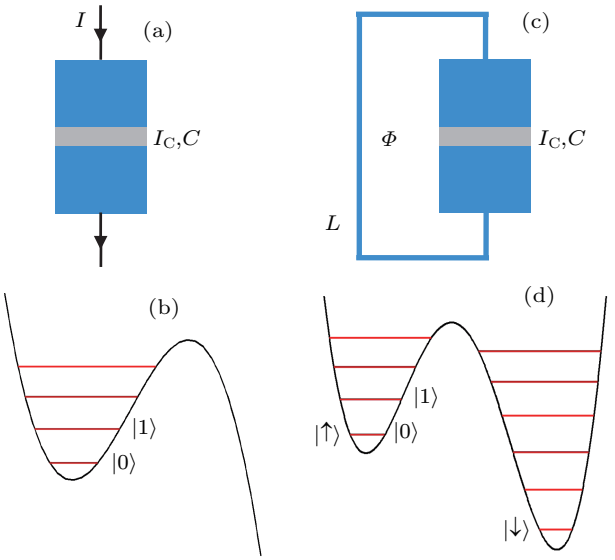


Fig. 1. (color online) (a) Current-biased Josephson junction as a phase qubit and (b) its potential and energy levels. (c) and (d) Corresponding ones of the rf-SQUID-type phase qubit, which can also be operated as a flux qubit.

One can also use the magnetic flux Φ as the experimentally controllable parameter instead of I by using an rf-SQUID type configuration shown in Fig. 1(c). In this case, when the flux quantization condition Eq. (2) is taken into account, the system is then governed by

$$m\ddot{\phi} + (m/RC)\dot{\phi} = -\partial U(\phi)/\partial\phi, \tag{5}$$

$$U(\phi) = (\Phi_0^2/2L)[(\phi - \phi_e)^2 - (\beta/2\pi^2)\cos(2\pi\phi)], \tag{6}$$

in which $\phi = \Phi/\Phi_0$ and $\phi_e = \Phi_e/\Phi_0$ are the normalized total and external fluxes, respectively, and $m = \Phi_0^2 C$, $\beta = 2\pi L I_c/\Phi_0$ with the loop inductance L. It can be verified that when $\beta > 1$, the two lowest potential wells are symmetric when ϕ_e=1/2, which correspond to the two circulating currents of opposite directions in the loop. Changing ϕ_e away from 1/2 will tilt the potential wells, and also the barrier height and level spacing. Figure 1(d) shows the case when $\phi_e \neq 1/2$, in which the bottom two states in the left well can be used as the phase qubit states. The state manipulation is similar to the situation discussed above but the state readout is realized by a SQUID detector which monitors the circulating current direction change upon tunneling out from the left to the right potential well. The rf-SQUID type phase qubit has been developed and studied extensively by the UCSB group.[16–19]

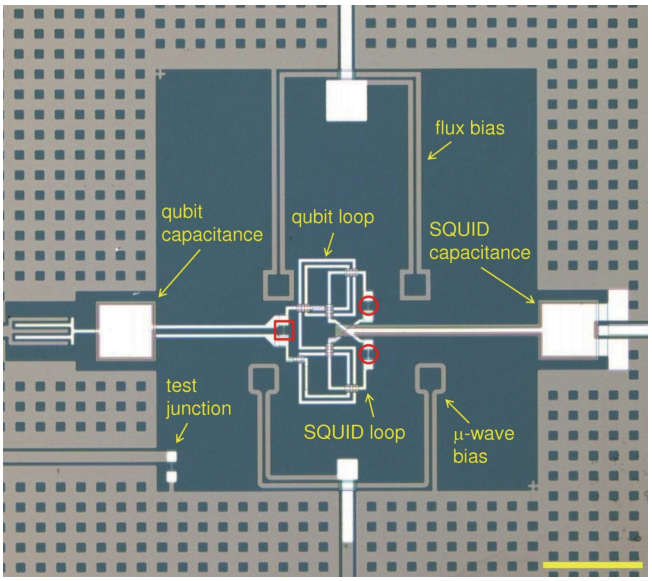


Fig. 2. (color online) Optical microscope image of an rf-SQUID-type phase qubit. The red open square and circles enclose the shadow evaporated junctions of the qubit and detector SQUID, respectively. The bar at the bottom-right corner indicates a length of 100 μm. (Figure reproduced with permission from Ref. [20]).

Figure 2 shows the photograph of an rf-SQUID-type phase qubit fabricated using the multilayer process.[20] The device layout is similar to the design developed in Refs. [18] and [19] but the fabrication process is changed to include the shadow evaporation of the Josephson junctions. The design looks a bit complicated largely due to the effort to minimize the crosstalks among different parts of the circuits. In the design, the SQUID detector contains three Josephson junctions, where a small junction is in parallel with two larger ones connected in series whose critical current is 1.7 times that of the small one. The advantage of the 3-junction dc-SQUID

is that it requires no external flux bias for the operation as a magnetometer. One is able to modulate the flux sensitivity and turn on (off) the coupling during qubit measurement (operation).[18]

It can be seen from Fig. 1(d) that the qubit can be operated as a flux type device if the two bottom states $|\uparrow\rangle$ and $|\downarrow\rangle$ in two different potential wells are used.[21] The two states correspond to the currents circulating in the qubit loop with different polarity. This rf-SQUID type flux qubit, which differs from the persistent-current flux qubit, is the key component in the quantum annealer built by the D-Wave Systems Inc., which we will discuss in further detail below.

2.2. Charge and transmon qubits

Figure 3(a) shows the schematic of a charge qubit. Clearly, the Hamiltonian of the system can be written as $H = (Q - C_g V_g)^2/2(C + C_g) - E_J \cos\varphi$, with $Q = 2en$ being the charge on the island separated by the tunneling barrier and the capacitor C_g, where C_g and V_g are the gate capacitance and gate voltage, respectively. Denoting the charging energy scale $E_C = e^2/2(C + C_g)$, the Hamiltonian becomes

$$H = 4E_C(n - n_g)^2 - E_J \cos\varphi, \tag{7}$$

where $n_g = C_g V_g/2e$. The charge qubit works in the regime $E_C \gg E_J$ so the charging energy dominates. Figure 3(b) shows the energy versus n_g in this case, calculated using the approach given in Ref. [22]. It can be seen that the main feature in the large scale is a series of parabolas for different integers of n. At the (half) integers of n_g, the energy of the neighboring parabolas is degenerate so the Josephson tunneling mixes the states resulting in the lifting up of degeneracy. The lowest two hybridized states near a given half integer n_g with level separation $\sim E_J$ are used as the qubit states. Quantum oscillations in the qubits were first observed by Nakamura *et al.* with a coherence time of the order of ns.[3]

In the opposite regime where $E_C \ll E_J$, the energy spectrum is quite different and becomes almost flat, as can be seen in Fig. 3(c). Koch *et al.* proposed a new type of qubit operating in this regime, which was termed "transmon".[23–25] The transmon qubit has an obvious advantage that it is much less sensitive to the charge noise due to the flat spectrum and therefore has a longer coherence time as compared to the charge qubit. A flat spectrum also means that one does not need to tune n_g as in the case for the charge qubit. The lowest two energy levels are used as the qubit levels as is depicted in Fig. 3(d). Experimentally, the transmon qubit can be built by simply connecting a capacitor in parallel with a Josephson junction, namely by shorting the voltage source V_g in Fig. 3(a). In this case, the transmon qubit is similar to the phase qubit in Fig. 1(a) with identical Hamiltonian when $I = 0$ and the junction is connected in parallel with a capacitor.

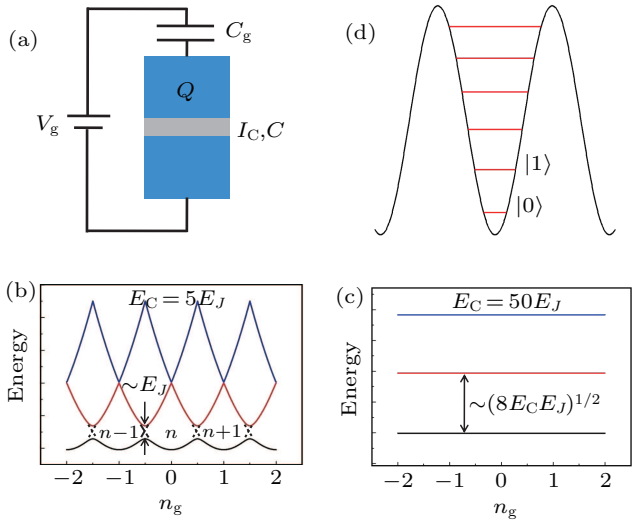


Fig. 3. (color online) (a) The charge qubit schematic. The transmon qubit can be derived by shorting the gate voltage source ($V_g = 0$). Energy spectra in the cases of $E_C \gg E_J$ (b) and $E_C \ll E_J$ (c). (d) Potential well and energy levels of the transmon qubit.

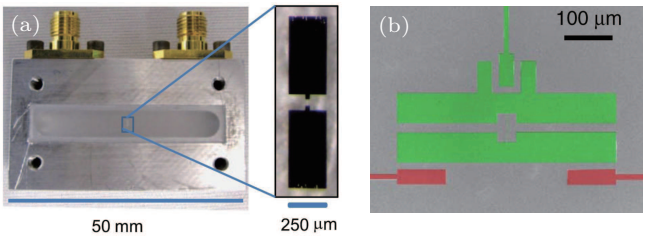


Fig. 4. (color online) Optical microscope images of three-dimensional (3D) (a) and two-dimensional (2D) (b) transmon qubits. Figures reproduced with permission from Refs. [26] and [27], respectively.

Figure 4(a) shows a transmon qubit imbedded in three-dimensional (3D) cavity resonator.[26] The enlarged part is the qubit with a shadow evaporated junction at the center and the two large pads being the capacitor electrodes on one hand and making the coupling to the resonator on the other. The resonator coupled with the qubit is used to detect the qubit states and also protect the qubit from the environmental electromagnetic noises (see below). Coherence times as long as $T_1 = 60$ μs, $T_2 = 20$ μs, and $T_{echo} = 25$ μs were measured in the energy relaxation, Ramsey, and spin-echo experiments, respectively. Figure 4(b) shows a recently reported two-dimensional (2D) transmon qubit,[27] where the two large horizontal pads are the capacitor electrodes with the junction located at the center. Two smaller pads at the bottom are used for the capacitive couplings to the other qubits, while the small pad at the top is leading to a resonator that is used for both the microwave excitation and qubit state measurement. Coherence times of T_1 and T_{echo} around 30 μs and 20 μs were demonstrated experimentally.[28]

A new qubit design named Xmon[29] was developed by the UCSB group based on the earlier planar transmon qubit.[23–25] As can be seen in Fig. 5, the Xmon qubit has a cross shape with its four arms connected to XY control, Z control, coupling to other qubit, and the resonator, which is used for the qubit state readout. The extreme flexibility makes the

Xmon qubit suitable for various studies of the coupled qubit system. The energy relaxation time T_1 above 40 μs was experimentally demonstrated in these devices.

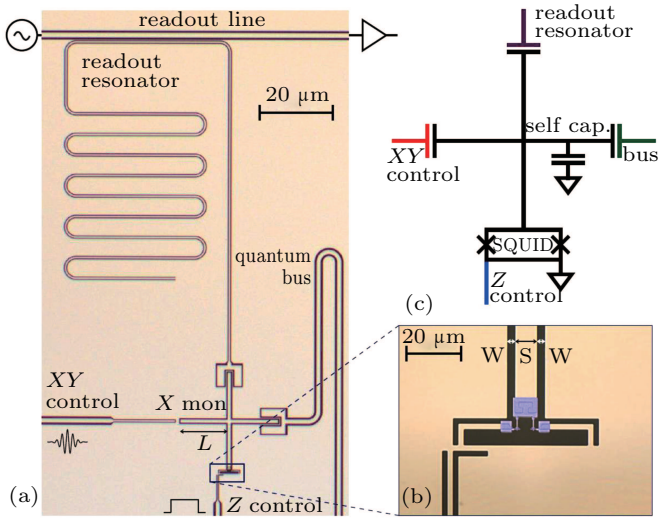


Fig. 5. (color online) (a), (b) Optical micrographs of an Xmon qubit. (c) The electrical circuit of the qubit. Figure reproduced with permission from Ref. [29].

The qubit state measurement of the transmon and Xmon devices is realized by coupling them to a resonator, e.g., to a 3D resonator as shown in Fig. 4(a) or to a 2D coplanar waveguide (CPW) resonator as shown in Figs. 4(b) and 5(a). This qubit-resonator circuit quantum electrodynamics (QED) architecture enables the quantum nondemolition measurement for the qubit state,[30–32] which will be discussed in Section 3.

2.3. Persistent-current flux qubits

The persistent-current flux qubit was first proposed by Mooij *et al.*, which had its original structure as shown in Fig. 6(a) in the absence of the shunting capacitor C_S.[33,34] The qubit is formed with a superconducting loop interrupted by three Josephson junctions, with one junction a factor of α smaller in area than the other two. The junctions contribute much inductance and a small loop with negligible inductance is used, making it less sensitive to the external noise. Considering the energy of the form $1-\cos\varphi$ stored in the each junction,[15] the qubit potential can be written as:

$$U(\varphi_1,\varphi_2) = E_J(2-\cos\varphi_1-\cos\varphi_2) + \alpha E_J[1-\cos(2\pi f+\varphi_1-\varphi_2)], \quad (8)$$

in which $\varphi_{1,2}$ are the phase differences across the two larger junctions, and f is the magnetic flux frustration defined by $\varphi_1-\varphi_2+\varphi_3=-2\pi f$ with φ_3 being the phase difference of the smaller junction.

The general feature of $U(\varphi_1,\varphi_2)$ is plotted in Fig. 6(b). A double-well potential can be seen more clearly in panel (c), which results from a cut along the red line in panel (b) and appears asymmetric as the external flux bias $\Phi_e \neq \Phi_0/2$. The barrier height separating the two wells can be adjusted by changing α. Usually, α is in the range of 0.5–0.7 or below so that quantum tunneling occurs leading to the hybridization of the $|\uparrow\rangle$ and $|\downarrow\rangle$ states near their degeneracy point of $\Phi_e=\Phi_0/2$. The $|\uparrow\rangle$ and $|\downarrow\rangle$ states correspond to the currents circulating in the qubit loop with opposite directions and the two hybridized states are used as the qubit states.

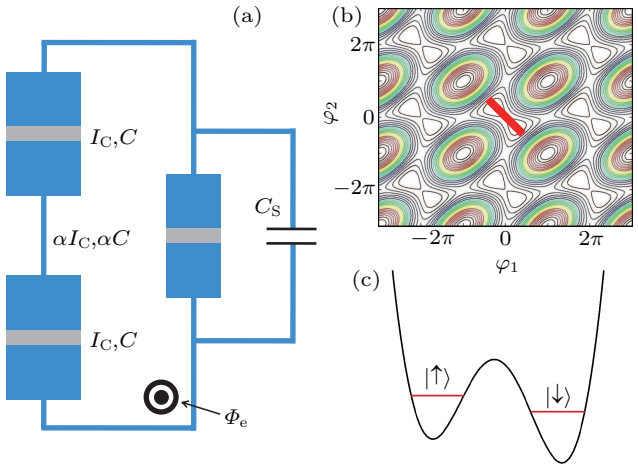


Fig. 6. (color online) (a) A persistent-current flux qubit schematic. (b) A contour plot of the potential in Eq. (8). (c) The potential along the direction indicated by a red line in panel (b) when $\Phi_e \neq \Phi_0/2$. States in the two potential wells correspond to the currents circulating in the qubit loop with opposite polarities.

The probability of observing $|\uparrow\rangle$ or $|\downarrow\rangle$ state is different in the qubit ground and excited states when it is not biased at degeneracy point. Hence one may detect the qubit states using a dc-SQUID that monitors the loop flux difference between the two states.[6] At the degeneracy point, the probability of observing the two basis states is the same and there is no net current difference between the ground and excited states. In this case, it is possible to determine the qubit state by applying a fast flux bias pulse to adiabatically shift the qubit to a non-degeneracy point. It is also possible to detect the quantum state using the inductive method similar to that used for transmon and Xmon.[35–37] This method, which can work at the degeneracy point, has the advantage of avoiding the voltage state of readout dc-SQUID so its back action to the qubit is minimized.

One can replace the small junction with a dc-SQUID, called α loop, which allows the modulation of the critical current and the qubit level spacing (or gap) by external flux. This type of gap tunable flux qubit has been demonstrated by several groups.[38–40] Using this design, Fedorov *et al.* observed macroscopic quantum coherence oscillations[41] and Zhu *et al.* coherently coupled a flux qubit to the nitrogen–vacancy (NV) centers.[42]

Compared with the phase and transmon (Xmon) qubits, the flux qubit is advantageous in that it has a much larger anharmonicity. On the other hand, You *et al.*[43] proposed a design to increase the qubit coherence time by shunting the small

junction with a capacitor C_S to suppress the charge noise, as is shown in Fig. 6(a). Systematic works by the MIT and UC Berkeley groups showed a significant increase in the coherence times, with T_1 reaching 40 μs–50 μs and T_2 approaching $2T_1 \sim 80$ μs.[44] The devices also showed strong anharmonicity of 500 MHz–700 MHz and the improved sample reproducibility.

One important feature of the flux qubits reported in Ref. [44] is the reduced α value. It is shown that for α greater than 0.5 the coherence time is much shorter. When α is decreased below 0.5, the double well feature of the qubit potential weakens with decreasing barrier height and the flux qubit becomes similar to the transmon qubit. It is reported that the flux qubits with the modified design eliminating the quadratic term show the T_1 values around 80 μs (see the device in Fig. 7).[45] Recent work also shows that by implementing a pumping sequence to reduce the number of unpaired quasiparticles in close proximity to the device, a threefold enhancement in qubit relaxation times and a comparable reduction in coherence variability can be achieved.[46]

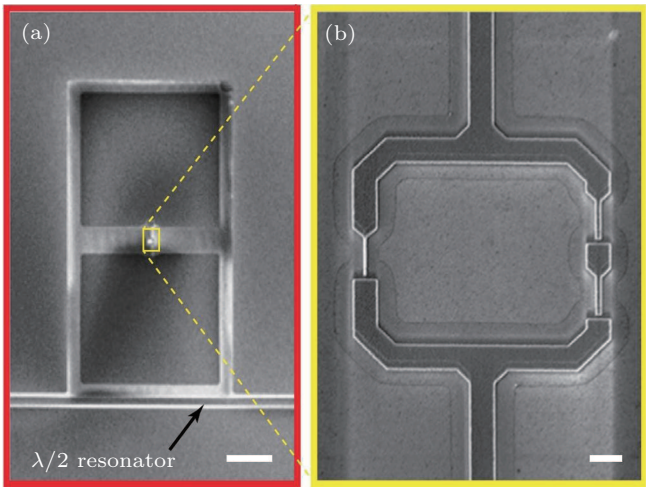


Fig. 7. (color online) (a), (b) Microscope images of a persistent-current qubit. The horizontal $\lambda/2$ CPW resonator at the bottom in panel (a) couples to the qubit for the qubit state measurement. Figure reproduced with permission from Ref. [45].

3. Quantum nondemolition measurement

The transmon qubit was derived from the charge qubit by the Yale group,[23–25] along with the technique of quantum nondemolition measurement of the qubit state based on the circuit QED architecture.[30–32] In the circuit QED framework, the Hamiltonian of the coupled qubit-resonator system has the Jaynes–Cummings form

$$H = \hbar\omega_{\rm r}(a^{\dagger}a + 1/2) + (\hbar\omega_{\rm q}/2)\sigma^{z} + \hbar g(a^{\dagger}\sigma^{-} + \sigma^{+}a), \quad (9)$$

where $\omega_{\rm r}$, $\omega_{\rm q}$, and g are the resonator frequency, qubit transition frequency, and resonator-qubit coupling strength, respectively. $a^{\dagger}$ and a are the photon creation and annihilation operators, $\sigma^{\pm} = (\sigma^{x} \pm {\rm i}\sigma^{y})/2$ are the qubit raising and lowering operators defined by the Pauli matrices in the usual sense, and we have ignored the cavity decay and qubit decoherence terms. An interesting result is that by performing a unitary transformation H can be reduced to

$$UHU^{\dagger} = \hbar[\omega_{\rm r} + (g^2/\Delta)\sigma^{z}]a^{\dagger}a + (\hbar/2)[\omega_{\rm q} + (g^2/\Delta)]\sigma^{z}, \quad (10)$$

in which $\Delta = \omega_{\rm q} - \omega_{\rm r}$ is the resonator-qubit detuning and

$$U = \exp[(g/\Delta)(a\sigma^{+} - a^{\dagger}\sigma^{-})].$$

This result indicates that the qubit level spacing is influenced by the number of photons in the resonator: The Stark shift term $2a^{\dagger}ag^2/\Delta$ and the Lamb term g^2/Δ. The result can also be viewed as a dispersive shift of the resonator frequency by $\chi\sigma^{z}$ with $\chi \equiv g^2/\Delta$.

Hence the qubit state will influence the resonator frequency. In other words, one is able to detect the qubit state by measuring the resonator transmission (or reflection) property. In a further analysis, Gambetta *et al.* considered the cavity decay rate κ, the qubit energy relaxation rate γ_1, and dephasing rate γ_φ. Under certain approximations, the master equation can be solved analytically to obtain the steady-state solutions of the photonic coherent states in the cavity:[32]

$$\alpha^{s}_{\pm} = -{\rm i}\varepsilon_{\rm rf}/(\kappa/2 \pm {\rm i}\chi + {\rm i}\Delta_{\rm r}), \quad (11)$$

where $\varepsilon_{\rm rf}$ is the amplitude of the measurement microwave in the cavity and $\Delta_{\rm r} = \omega_{\rm r} - \omega_{\rm rf}$ is its detuning with respect to the resonator frequency. The stationary average number of photons in the cavity is thus

$$\bar{n}_{\pm} = |\,\alpha^{s}_{\pm}\,|^2 = \varepsilon^2_{\rm rf}/[\kappa^2/4 + (\Delta_{\rm r} \pm \chi)^2]. \quad (12)$$

In Eqs. (11) and (12), the "–" and "+" correspond to results when the qubit is in the ground and excited states, respectively. Since experimentally one usually has $\chi \gg \kappa$, equation (12) indicates that the cavity response will exhibit two peaks located at $\omega_{\rm r} \pm \chi$ corresponding to the qubit ground and excited states. Figure 8 shows the experimental results measured from a coupled transmon qubit-resonator system.[47] At low microwave power (near the bottoms of the two panels), peaks at different locations can be clearly seen in panels (a) and (b) with the qubit states prepared in the ground and excited states, respectively.

The qubit states can also be detected by the phase difference of the cavity coherent states given in Eq. (11). Namely one can apply the measurement microwave with frequency $\omega_{\rm rf} = \omega_{\rm r}$ such that $\Delta_{\rm r} = 0$. In this way, the states $\alpha^{s}_{\pm}$ have the phases of $\pm\theta = \pm\tan^{-1}(2\chi/\kappa)$, which tend to $\pm 90^{\circ}$ when $\chi \gg \kappa$.

The quantum nondemolition measurement of the qubit state can be realized using the above technique if the microwave power is kept low so that the average photon number $\bar{n}_{\pm}$ is small.[30] On the other hand, we can see in Fig. 8 that

as the measurement microwave power increases, the peaks developed with the particular qubit state become stronger and widen at the same time. If we look at the frequency $\omega_{\rm rf} = \omega_{\rm r} = 9.07$ GHz, the cavity response or transmission becomes extremely high above certain critical microwave power that depends sensitively on the qubit state. The inset shows the response versus the microwave power when the qubit is in the ground and excited states. This result is due to the nonlinearity of the Jaynes–Cummings interaction of the qubit and cavity,[48,49] which can be used conveniently for the qubit state measurement[47] provided the state demolition is not a concern.

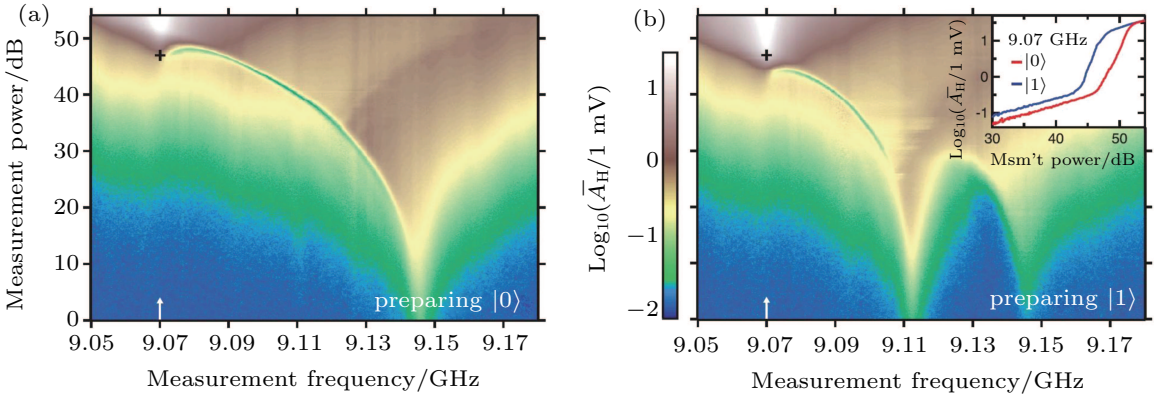


Fig.8. (color online) Cavity responses for qubit ground (a) and excited (b) states. Inset: Response at 9.07 GHz versus input power. Figure reproduced with permission from Ref. [47].

The quantum nondemolition measurement for the qubit state based on the circuit QED setup is advantageous in many ways compared to that using a dc-SQUID. It does not destroy the quantum state of the qubit and the single-shot measurement can be realized using the quantum-limited Josephson parametric amplifiers.[50–55] The technique is also applied for the phase[56] and flux[35–37,45] qubit devices.

4. Improving qubit coherence

Raising the quantum coherence time is among the key issues in the superconducting qubit studies, and enormous efforts considering various possible mechanisms causing the qubit decoherence have been made.[57] One continuous effort has been to reduce the dielectric loss from the qubit surrounding materials that are always present, such as the substrate, the insulation layers, and the oxidized tunnel barrier or metal surface.[17] Dielectric loss at low temperature is believed to arise from the two-level states (TLS), which can always be seen in the phase qubit with large-area Josephson junctions. TLS can be greatly reduced or absent when the junction size is reduced down to the submicron regime,[20] which may result from the annealing of the defects by stress relieving of the small-sized junctions, or can be understood from the simple statistical point of view.[57] Smaller junctions combined with shunt capacitors are therefore used for the phase qubit. It is experimentally demonstrated that parallel plate capacitors with low dielectric loss can lead to the improvement of the energy relaxation times by a factor of 20.[17]

Early experiments of the charge qubits only demonstrate ns-scale coherence times. As discussed above, a significant progress is from the charge qubit derived transmon,[23] which is immune to the $1/f$ charge noise thus removing the leading source of dephasing resulting in increased μs-scale coherence times.[58] A further important improvement comes from the understanding of the resonator in modifying the qubit electromagnetic environment.[23,59] The idea behind this is the so-called "Purcell effect". Namely, the qubit spontaneous emission can be effectively suppressed by coupling it to a resonator which greatly modify the modes and density of states of the electromagnetic field in the external circuitry.[59] The reduced spontaneous emission effectively enhance the qubit energy relaxation times.

Transmon (Xmon) and persistent-current flux qubits only need modest shunt capacitance compared to the phase qubit. In Fig. 4, Fig. 5(a), and Fig. 7(a), the shunt capacitors are formed by two electrodes with the substrate as the insulation layer between them. This makes it easier to reduce the dielectric loss if the low-loss substrate is used and the substrate surface is carefully treated. Dielectric losses of the 2D resonators, together with the qubits as a whole, have been carefully studied in the past decade.[60–70] A convenient concept, called "participation ratio",[23,60] is often used. The participation ratio is defined as the electric field energy stored in the lossy material divided by the total electric field energy stored in the entire device. It is found that the participation ratio and dielectric loss decrease with the increasing device feature size (footprint),[60,61,66,67] which provides evidence that the loss is interface or surface limited.[60] Some experiments indicate that the dominant loss comes from the substrate–air and substrate–metal interfaces while the metal–air interface plays a lesser role.[68,71] The 3D transmon is advantageous in this respect since the sizes of the devices are larger, thus lowering the participation ratio and loss from interfaces. The participation ratio in 3D transmon is carefully studied in Refs. [71] and [72].

In addition to the advances discussed above, namely re-

ducing the dielectric loss, designing qubits immune to the external noises, and modifying the electromagnetic environment, we mention also the other efforts such as improving materials and fabrication techniques,[62,65,67,69] and improving filtering and shielding against stray radiation that causes quasiparticle dissipation.[73] All these efforts have incrementally and collectively raised qubit coherence times up to the present level of 10 μs–100 μs and beyond, in the devices such as those shown in Figs. 4, 5, and 7.

5. Experiments with superconducting qubits

We have discussed various types of the superconducting qubits, their basic principles, operations, and improvements. In this section, we will have a brief look into the rich ongoing research works with the superconducting qubits.

5.1. Qubit coupling and logic gates

Superconducting qubits have many types as discussed previously and there are also many ways of coupling them together, including capacitive and inductive couplings, and couplings via Josephson junctions and resonators.[9,10] Single- and multi-qubit quantum gate operations, required for the universal gate-based quantum computation, have been experimentally demonstrated with improving fidelity, starting from the early years after finding the qubit coherence. Single qubit logic operations of different angle rotations about the x, y, and z axes of the Bloch sphere are performed, for instance, in the quantronium,[74] phase,[75] and transmon[76] qubits, which suffice the usual single qubit phase gate, phase-slip gate, NOT gate, and Hadamard gate. Two qubit logic operations such as controlled-NOT (cNOT) gates are realized in charge[77] and persistent-current qubit.[77,78] The square root of i-SWAP gate is also realized in the phase qubit.[79] The three qubit Toffoli gates (ccNOT) are successfully demonstrated in transmon qubits.[80,81] Universal gate sets are proposed[82] and are experimentally implemented and characterized.[83]

5.2. Quantum physics on chip

Superconducting circuits and qubits behave quantum mechanically on a macroscopic scale with the system parameters conveniently controllable, which provide an excellent tool for the studies of quantum physics, atomic physics, and quantum optics. There are vast published works in the literature, out of which we only mention a few: (i) Resonant escapes and bifurcation phenomena of nonlinear systems under strong driving.[84,85] (ii) Macroscopic quantum tunneling in cuprate materials and phase diffusion in the quantum regime.[86,87] (iii) Quantum stochastic synchronization in dissipative quantum systems.[88] (iv) Landau–Zener–Stückelberg interference and the precise control of quantum states in the tripartite system.[89,90] (v) Topological phase diagram and phase transitions in interacting quantum systems.[91] (vi) A Schröinger cat living in two boxes.[92] (vii) The Autler–Townes splitting phenomena.[93–97] (viii) The stimulated Raman adiabatic passage and coherent population transfer.[98,99] (ix) The electromagnetically induced transparency, a phenomenon similar to Autler–Townes splitting but physically distinct.[100,101] (x) Resonance fluorescence and correlated emission lasing.[102,103]

5.3. Adiabatic quantum computing

Adiabatic quantum computing or quantum annealing was proposed as a heuristic technique for quantum enhanced optimization nearly two decades ago.[104–107] This architecture, known to be equivalent to the standard gate-based quantum computation,[108,109] is simpler and provides a more practical approach for applications in the near term. The first superconducting quantum annealing processors were built by the D-Wave Systems Inc.[110,111] based on the rf-SQUID type flux qubits[21] and the Nb-junction technology.[112,113] The D-Wave One, D-Wave Two, D-Wave 2X, and D-Wave 2000Q machines have become available in the years 2011, 2013, 2015, and 2017 with coupled 128, 512, 1024, and 2048 qubits, respectively. Although superconducting quantum annealing has received much attention both academically and industrially, a consensus on some physics and its potential for achieving optimization algorithm has not been reached. For more recent studies the readers are referred to the works in Refs. [114]–[117] by Google Inc. and D-Wave Systems Inc., for instance, and references therein.

5.4. Quantum simulation

Quantum simulation, namely using a controllable quantum system to simulate another quantum system, was first proposed by Richard Feynman and was envisioned as the main application of a quantum computer.[118,119] Quantum simulation has two types: The digital quantum simulation and the analog quantum simulation. The former simulates a quantum system by dividing the time evolution of a Hamiltonian, written as a sum of local terms, into small intervals which can be realized by a sequence of qubit gate operations.[120] In the analog quantum simulation, the Hamiltonian of the system to be simulated is directly mapped onto the Hamiltonian of the simulator that can be experimentally controlled. Quantum simulation may find a variety of applications ranging from atomic physics, chemistry, condensed-matter physics, cosmology, and high-energy physics.[13,121,122]

In condensed-matter physics, in particular, Las Heras *et al.* proposed the implementation of digital quantum simulators for the Heisenberg and frustrated Ising models[123] and Fermi–Hubbard models,[124] which were experimentally validated in Refs. [125] and [126], respectively. Digital and analog simulations of the Fermi–Hubbard models were discussed in Refs. [127]–[129]. Quantum emulation of creating anyonic excitations was also achieved experimentally by dynamically generating the ground and excited states of the toric code model.[130] There are still many proposals for the

analog simulators put forward which need experimental tests: Transverse-field Ising or other spin models;[131–133] Holstein molecular-crystal model exhibiting electron–phonon-induced small-polaron formation;[134,135] multi-connected Jaynes–Cummings lattice model with Mott insulator-superfluid-Mott insulator phase transition;[136,137] pairing Hamiltonians built from nearest-neighbor-interacting qubits;[138] quantum emulation of spin systems with topologically protected ground states.[139,140]

5.5. Quantum computation

Devoret and Schoelkopf discussed some key stages in the development of a practical superconducting quantum computer.[12] Briefly, one needs the single and multiple *physical* qubits which satisfy the first five DiVincenzo criteria: A well-defined quantum two-state system, the ability to initialize the state, long (relative) coherence times, single- and two-qubit logic gate operations, and the state measurement capability.[141] This is followed by moving to the *logical* qubits and memories, which have much longer coherence times, by means of quantum error correction. Finally, gate operations on single and multiple logical qubits are realized to reach the ultimate goal of fault-tolerant quantum computation.

Quantum error correction is of crucial importance for the realization of quantum computing and has received much attention.[28,81,142,143] In order to perform error correction, the fidelity of gate operation must be above certain threshold, which can be measured by the double π-pulse, quantum process tomography, and randomized benchmarking methods.[76] Barends *et al.* showed that, using a 5-qubit array an average single-qubit gate fidelity of 99.92% and a two-qubit gate fidelity of up to 99.4% could be achieved.[144] This places the quantum computing at the fault tolerance threshold for surface code error correction. The same authors also reported the protection of classical states from environmental bit-flip errors and demonstrated the suppression of these errors with increasing system size on a 9-qubit array.[142] Meanwhile, Chow *et al.* reported a quantum error detection protocol on a two-by-two planar qubit lattice.[27] The protocol could detect both bit-flip error and phase-flip error, making it possible to detect an arbitrary quantum error.[28] Ofek *et al.* adopted a different approach to implement a full quantum error correction by using real-time feedback for encoding, monitoring naturally occurring errors, decoding, and correcting. They demonstrated a quantum error correction system that reached the break-even point (i.e., enhanced lifetime of the encoded information) by suppressing the natural errors due to energy loss for a qubit logically encoded in superpositions of coherent states of a superconducting resonator.[143]

For a multiple qubit circuit, the demonstration of quantum entanglement and quantum algorithms is an important step toward quantum computing. Among many other works, Song *et al.* demonstrated the production and tomography of genuinely entangled Greenberger–Horne–Zeilinger (GHZ) states with up to 10 qubits that connect to a common bus resonator in a superconducting circuit.[145] Grover search and Deutsch–Jozsa quantum algorithms[146] as well as solving linear equations[147] were also demonstrated. Furthermore, Riste *et al.* showed the quantum advantage in performing a machine learning algorithms using a 5-qubit superconducting processor.[148]

While most present studies are performed on the devices of which all components are arranged on chip in a planar fashion, efforts have been made to make devices that have components distributed on different chips stacked vertically in order to accommodate more qubits and also reduce interference and cross talk between different qubits.[149–151] Similar 3D integration is well developed for the semiconductor integrated circuits. However, the application of the technology to the superconducting circuits and qubits is not straightforward and requires further investigation. Of particular concern, quantum coherence could be seriously suppressed by the requisite processing steps and the progress in the coming years on this issue will be crucial for building chips containing around 100 qubits and above.

6. Summary and perspective

In the past two decades, tremendous progress has been made in the studies of superconducting circuits and qubits. Most notably, the quantum coherence times have been increased by five orders of magnitude up to the range of 10 μs–100 μs in the devices such as the 2D and 3D transmon qubits, the Xmon qubits, and the persistent-current flux qubits. These devices have improved designs that offer better controls over the qubit fabrication, manipulation, measurement as well as multi-qubit coupling. Research works in many aspects are underway, which may finally lead to the physical implementation of quantum computing. At the present stage, it is encouraging to see that the studies so far have demonstrated most of the basic properties and functionalities required for building a quantum computer. On the other hand, we are entering a further stage with more complex quantum systems in which new fundamental physical and technical problems need to be solved and answered. Before the ultimate goal of quantum computing is reached, fruitful results in the studies of quantum physics, atomic physics, quantum optics, quantum annealing, and quantum simulation would be expected.

References

[1] Devoret M H, Esteve D, Urbina C, Martinis J, Cleland A and Clarke J 2002 in *Exploring the quantum classical frontier: Recent advances in macroscopic phenomena*, eds. Friedman J R and Han Siyuan (New York: Nova Science Publishers)

[2] Han Siyuan 2002 in *Exploring the quantum classical frontier: Recent advances in macroscopic phenomena*, eds. Friedman J R and Han Siyuan (New York: Nova Science Publishers)

[3] Nakamura Y, Pashkin Y A and Tsai J S 1999 *Nature* **398** 6730

[4] Martinis John M, Nam S, Aumentado J and Urbina C 2002 *Phys. Rev. Lett.* **89** 117901

[5] Yu Yang, Han Siyuan, Chu Xi, Chu Shih-I and Wang Zhen 2002 *Science* **296** 889

[6] Chiorescu I, Nakamura Y, Harmans C J P M and Mooij J E 2003 *Science* **299** 1869

[7] Vion D, Aassime A, Cottet A, Joyez P, Pothier H, Urbina C, Esteve D, and Devoret M H 2002 *Science* **296** 886

[8] Makhlin Y, Schön G and Shnirman A 2001 *Rev. Mod. Phys.* **73** 357

[9] Wendin G and Shumeiko V S 2006 in *Handbook of Theoretical and Computational Nanotechnology*, ed. Rieth M and Schommers W (American Scientific Publishers)

[10] Clarke J and Wilhelm F K 2008 *Nature* **453** 1031

[11] You J Q and Nori F 2011 *Nature* **474** 589

[12] Devoret M H and Schoelkopf R J 2013 *Science* **339** 1169

[13] Georgescu I M, Ashhab S and Nori F 2014 *Rev. Mod. Phys.* **86** 153

[14] Wendin G 2016 arXiv: 1610.02208

[15] Tinkham M 1996 *Introduction to Superconductivity* (New York: McGraw-Hill)

[16] Simmonds R W, Lang K M, Hite D A, Nam S, Pappas D P and Martinis J M 2004 *Phys. Rev. Lett.* **93** 077003

[17] Martinis J M, Cooper K B, McDermott R, Steffen M, Ansmann M, Osborn K D, Cicak K, Oh S, Pappas D P, Simmonds R W and Yu C C 2005 *Phys. Rev. Lett.* **95** 210503

[18] Neeley M, Ansmann M, Bialczak R C, Hofheinz M, Katz N, Lucero E, O'Connell A, Wang H, Cleland A N and Martinis J 2008 *Phys. Rev. B* **77** 180508

[19] Martinis J M 2009 *Quantum Inf. Process.* **8** 81

[20] Su F F, Liu W Y, Xu H K, Deng H, Li Z Y, Tian Ye, Zhu X B, Zheng D N, Lv Li and Zhao S P 2017 *Chin. Phys. B* **26** 060308

[21] Friedman J R, Patel V, Chen W, Tolpygo S K and Lukens J E 2000 *Nature* **406** 43

[22] Devoret M H, Wallraff A and Martinis J M 2004 arXiv: cond-mat/0411174 (unpublished)

[23] Koch J, Yu T M, Gambetta J, Houck A A, Schuster D I, Majer J, Blais A, Devoret M H, Girvin S M and Schoelkopf R J 2007 *Phys. Rev. A* **76** 042319

[24] Houck A A, Schuster D I, Gambetta J M, Schreier J A, Johnson B R, Chow J M, Frunzio L, Majer J, Devoret M H, Girvin S M and Schoelkopf R J 2007 *Nature* **449** 328

[25] Majer J, Chow J M, Gambetta J M, Koch J, Johnson B R, Schreier J A, Frunzio L, Schuster D I, Houck A A, Wallraff A, Blais A, Devoret M H, Girvin S M and Schoelkopf R J 2007 *Nature* **449** 443

[26] Paik H, Schuster D I, Bishop L S, Kirchmair G, Catelani G, Sears A P, Johnson B R, Reagor M J, Frunzio L, Glazman L I, Girvin S M, Devoret M H and Schoelkopf R J 2011 *Phys. Rev. Lett.* **107** 240501

[27] Chow J M, Gambetta J M, Magesan E, Abraham D W, Cross A W, Johnson B R, Masluk N A, Ryan C A, Smolin J A, Srinivasan S J and Steffen M 2014 *Nat. Commun.* **5** 4015

[28] Córcoles A D, Magesan E, Srinivasan S J, Cross A W, Steffen M, Gambetta J M and Chow J M 2015 *Nat. Commun.* **6** 6979

[29] Barends R, Kelly J, Megrant A, Sank D, Jeffrey E, Chen Y, Yin Y, Chiaro B, Mutus J, Neill C, O'Malley P, Roushan P, Wenner J, White T C, Cleland A N and Martinis J M 2013 *Phys. Rev. Lett.* **111** 080502

[30] Blais A, Huang R S, Wallraff A, Girvin S M and Schoelkopf R J 2004 *Phys. Rev. A* **69** 062320

[31] Wallraff A, Schuster D I, Blais A, Frunzio L, Huang R S, Majer J, Kumar S, Girvin S M and Schoelkopf R J 2004 *Nature* **431** 162

[32] Gambetta J, Blais A, Schuster D I, Wallraff A, Frunzio L, Majer L, Devoret M H, Girvin S M and Schoelkopf R J 2006 *Phys. Rev. A* **74** 042318

[33] Mooij J E, Orlando T P, Levitov L, Tian L, van der Wal C H and Lloyd S 1999 *Science* **285** 1036

[34] Orlando T P, Mooij J E, Tian L, van der Wal C H, Levitov L S, Lloyd S and Mazo J J 1999 *Phys. Rev. B* **60** 15398

[35] Lupascu A, Verwijs C J M, Schouten R N, Harmans C J P M and Mooij J E 2004 *Phys. Rev. Lett.* **93** 177006

[36] Stern M, Catelani G, Kubo Y, Grezes C, Bienfait A, Vion D, Esteve D and Bertet P 2014 *Phys. Rev. Lett.* **113** 123601

[37] Orgiazzi J L, Deng C, Layden D, Marchildon R, Kitapli F, Shen F, Bal M, Ong F R and Lupascu A 2016 *Phys. Rev. B* **93** 104518

[38] Paauw F G, Fedorov A, Harmans C J P M and Mooij J E 2009 *Phys. Rev. Lett.* **102** 090501

[39] Zhu X B, Kemp A, Saito S and Semba K 2010 *Appl. Phys. Lett.* **97** 102503

[40] Schwarz M J, Goetz J, Jiang Z, Niemczyk T, Deppe F, Marx A and Gross R 2013 *New J. Phys.* **15** 045001

[41] Fedorov A, Macha P, Feofanov A K, Harmans C J P M and Mooij J E 2011 *Phys. Rev. Lett.* **106** 170404

[42] Zhu X B, Saito S, Kemp A, Kakuyanagi K, Karimoto S, Nakano H, Munro W J, Tokura Y, Everitt M S, Nemoto K, Kasu M, Mizuochi N and Semba K 2011 *Nature* **478** 221

[43] You J Q, Hu X D, Ashhab S and Nori F 2007 *Phys. Rev. B* **75** 140515

[44] Steffen M, Kumar S, DiVincenzo D P, Rozen J R, Keefe G A, Rothwell M B and Ketchen M B 2010 *Phys. Rev. Lett.* **105** 100502

[45] Yan F, Gustavsson S, Kamal A, Birenbaum J, Sears A P, Hover D, Gudmundsen T J, Rosenberg D, Samach G, Weber S, Yoder J L, Orlando T P, Clarke J, Kerman A J and Oliver W D 2016 *Nat. Commun.* **7** 12964

[46] Gustavsson S, Yan F, Catelani G, Bylander J, Kamal A, Birenbaum J, Hover D, Rosenberg D, Samach G, Sears A P, Weber S J, Yoder J L, Clarke J, Kerman A J, Yoshihara F, Nakamura Y, Orlando T P and Oliver W D 2016 *Science* **354** 1573

[47] Reed M D, DiCarlo L, Johnson B R, Sun L, Schuster D I, Frunzio L and Schoelkopf R J 2010 *Phys. Rev. Lett.* **105** 173601

[48] Boissonneault M, Gambetta J M and Blais A 2010 *Phys. Rev. Lett.* **105** 100504

[49] Bishop L, Ginossar E and Girvin S M 2010 *Phys. Rev. Lett.* **105** 100505

[50] Lin Z R, Inomata K, Oliver W D, Koshino K, Nakamura Y, Tsai J S and Yamamoto T 2013 *Appl. Phys. Lett.* **103** 132602

[51] Mutus J Y, White T C, Jeffrey E, Sank D, Barends R, Bochmann J, Chen Yu, Chen Z, Chiaro B, Dunsworth A, Kelly J, Megrant A, Neill C, O'Malley P J J, Roushan P, Vainsencher A, Wenner J, Siddiqi I, Vijay R, Cleland A N and Martinis J M 2013 *Appl. Phys. Lett.* **103** 122602

[52] Mutus J Y, White T C, Barends R, Chen Yu, Chen Z, Chiaro B, Dunsworth A, Jeffrey E, Kelly J, Megrant A, Neill C, O'Malley P J J, Roushan P, Sank D, Vainsencher A, Wenner J, Sundqvist K M, Cleland A N and Martinis J M 2014 *Appl. Phys. Lett.* **104** 263513

[53] Roy T, Kundu S, Chand M, Vadiraj A M, Ranadive A, Nehra N, Patankar M P, Aumentado J, Clerk A A and Vijay R 2015 *Appl. Phys. Lett.* **107** 262601

[54] White T C, Mutus J Y, Hoi I C, Barends R, Campbell B, Chen Yu, Chen Z, Chiaro B, Dunsworth A, Jeffrey E, Kelly J, Megrant A, Neill C, O'Malley P J J, Roushan P, Sank D, Vainsencher A, Wenner J, Chaudhuri S, Gao J and Martinis J M 2015 *Appl. Phys. Lett.* **106** 242601

[55] Macklin C, O'Brien K, Hover D, Schwartz M E, Bolkhovsky V, Zhang X, Oliver W D and Siddiqi I 2015 *Science* **350** 307

[56] Whittaker J D, da Silva F C S, Allman M S, Lecocq F, Cicak K, Sirois A J, Teufel J D, Aumentado J and Simmonds R W 2014 *Phys. Rev. B* **90** 024513

[57] Martinis J M and Megrant A 2014 arXiv: 1410.5793 (unpublished)

[58] Schreier J A, Houck A a, Koch J, Schuster D I, Johnson B R, Chow J M, Gambetta J M, Majer J, Frunzio L, Devoret M H, Girvin S M and Schoelkopf R J 2008 *Phys. Rev. B* **77** 180502

[59] Houck A A, Schreier J A, Johnson B R, Chow J M, Koch J, Gambetta J M, Schuster D I, Frunzio L, Devoret M H, Girvin S M and Schoelkopf R J 2008 *Phys. Rev. Lett.* **101** 080502

[60] Gao J, Daa M, Vayonakis A, Kumar S, Zmuidzinas J, Sadoulet B, Mazin B A, Day P K and Leduc H G 2008 *Appl. Phys. Lett.* **92** 152505

[61] Wang H, Hofheinz M, Wenner J, Ansmann M, Bialczak R C, Lenander M, Lucero Erik, Neeley M, O'Connell A D, Sank D, Weides M, Cleland A N and Martinisa J M 2009 *Appl. Phys. Lett.* **95** 233508

[62] Barends R, Vercruyssen N, Endo A, de Visser P J, Zijlstra T, Klapwijk T M, Diener P, Yates S J C and Baselmans J J A 2010 *Appl. Phys. Lett.* **97** 023508

[63] Wenner J, Barends R, Bialczak R C, Chen Yu, Kelly J, Lucero Erik, Matteo Mariantoni, A. Megrant, O'Malley P J J, Sank D, Vainsencher A, Wang H, White T C, Yin Y, Zhao J, Cleland A N and Martinis J M 2011 *Appl. Phys. Lett.* **99** 113513

[64] Sage Jeremy M, Bolkhovsky Vladimir, Oliver William D, Turek Benjamin and Welander Paul B 2011 *J. Appl. Phys.* **109** 063915

[65] Megrant A, Neill C, Barends R, Chiaro B, Chen Yu, Feigl L, Kelly J, Lucero Erik, Mariantoni Matteo, O'Malley P J J, Sank D, Vainsencher A, Wenner J, White T C, Yin Y, Zhao J, Palmstrøm C J, Martinis John M and Cleland A N 2012 *Appl. Phys. Lett.* **100** 113510

[66] Geerlings K, Shankar S, Edwards E, Frunzio L, Schoelkopf R J and Devoret M H 2012 *Appl. Phys. Lett.* **100** 192601

[67] Chang J B, Vissers M R, Córcoles A D, Sandberg M, Gao J, Abraham D W, Chow J M, Gambetta J M, Rothwell M B, Keefe G A, Steffen M and Pappas D P 2013 *Appl. Phys. Lett.* **103** 012602

[68] Quintana C M, Megrant A, Chen Z, Dunsworth A, Chiaro B, Barends R, Campbell B, Chen Yu, Hoi I C, Jeffrey E, Kelly J, Mutus J Y, O'Malley P J J, Neill C, Roushan P, Sank D, Vainsencher A, Wenner J, White T C, Cleland A N and Martinis J M 2014 *Appl. Phys. Lett.* **105** 062601

[69] Bruno A, de Lange G, Asaad S, van der Enden K L, Langford N K and DiCarlo L 2015 *Appl. Phys. Lett.* **106** 182601

[70] Gambetta J M, Murray C E, Fung Y K K, McClure D T, Dial O, Shanks W, Sleight J W and Steffen M 2017 *IEEE Trans. Appl. Supercond.* **27** 1700205

[71] Dial O, McClure D T, Poletto S, Keefe G A, Rothwell M B, Gambetta J M, Abraham D W, Chow J M and Steffen M 2016 *Supercond. Sci. Technol.* **29** 044001

[72] Wang C, Axline C, Gao Y Y, Brecht T, Chu Y, Frunzio L, Devoret M H and Schoelkopf R J 2015 *Appl. Phys. Lett.* **107** 162601

[73] Córcoles A D, Chow J M, Gambetta J M, Rigetti C, Rozen J R, Keefe G A, Rothwell M B, Ketchen M B and Steffen M 2011 *Appl. Phys. Lett.* **99** 181906

[74] Collin E, Ithier G, Aassime A, Joyez P, Vion D and Esteve D 2004 *Phys. Rev. Lett.* **93** 157005

[75] Lucero E, Hofheinz M, Ansmann M, Bialczak R C, Katz N, Neeley M, O'Connell A D, Wang H, Cleland A N and Martinis J M 2008 *Phys. Rev. Lett.* **100** 247001

[76] Chow J M, Gambetta J M, Tornberg L, Koch J, Bishop L S, Houck A A, Johnson B R, Frunzio L, Girvin S M and Schoelkopf R J 2009 *Phys. Rev. Lett.* **102** 090502

[77] Yamamoto T, Pashkin Yu A, Astafiev O, Nakamura Y and Tsai J S 2003 *Nature* **425** 941

[78] Plantenberg J H, de Groot P C, Harmans C J P M and Mooij J E 2007 *Nature* **447** 836

[79] Bialczak R C, Ansmann M, Hofheinz M, Lucero E, Neeley M, O'Connell A D, Sank D, Wang H, Wenner J, Steffen M, Cleland A N and Martinis J M 2010 *Nat. Phys.* **6** 409

[80] Fedorov A, Steffen L, Baur M, da Silva M P and Wallraff A 2012 *Nature* **481** 170

[81] Reed M D, DiCarlo L, Nigg S E, Sun L, Frunzio L, Girvin S M and Schoelkopf R J 2012 *Nature* **482** 382

[82] Rigetti C, Blais A and Devoret M 2005 *Phys. Rev. Lett.* **94** 240502

[83] Chow J M, Gambetta J M, Córcoles A D, Merkel S T, Smolin J A, Rigetti C, Poletto S, Keefe G A, Rothwell M B, Rozen J R, Ketchen M B and Steffen M 2012 *Phys. Rev. Lett.* **109** 060501

[84] Yu H F, Zhu X B, Peng Z H, Cao W H, Cui D J, Tian Ye, Chen G H, Zheng D N, Jing X N, Lu Li, Zhao S P and Han S 2010 *Phys. Rev. B* **81** 144518

[85] Yu H F, Zhu X B, Ren J K, Peng Z H, Cui D J, Deng H, Cao W H, Tian Ye, Chen G H, Zheng D N, Jing X N, Lu Li and Zhao S P 2013 *New J. Phys.* **15** 095006

[86] Li S X, Qiu W, Han S, Wei Y F, Zhu X B, Gu C Z, Zhao S P and Wang H B 2007 *Phys. Rev. Lett.* **99** 037002

[87] Yu H F, Zhu X B, Peng Z H, Tian Ye, Cui D J, Chen G H, Zheng D N, Jing X N, Lu Li, Zhao S P and Han S 2011 *Phys. Rev. Lett.* **107** 067004

[88] Xue G M, Gong M, Xu H K, Liu W Y, Deng H, Tian Ye, Yu H F, Yu Y, Zheng D N, Zhao S P and Han S 2014 *Phys. Rev. B* **90** 224505

[89] Sillanpää M, Lehtinen T, Paila A, Makhlin Y and Hakonen P 2006 *Phys. Rev. Lett.* **96** 187002

[90] Sun G, Wen X, Mao Bo, Chen J, Yu Y, Wu P and Han S 2010 *Nat. Commun.* **1** 51

[91] Roushan P, Neill C, Chen Yu, Kolodrubetz M, Quintana C, Leung N, Fang M, Barends R, Campbell1 B, Chen Z, Chiaro B, Dunsworth A, Jeffrey E, Kelly J, Megrant A, Mutus J, O'Malley P J J, Sank D, Vainsencher A, Wenner J, White T, Polkovnikov A, Cleland A N and Martinis J M 2014 *Nature* **515** 241

[92] Wang C, Gao Y Y, Reinhold P, Heeres R W, Ofek N, Chou K, Axline C, Reagor M, Blumoff J, Sliwa K M, Frunzio L, Girvin S M, Jiang L, Mirrahimi M, Devoret M H and Schoelkopf R J 2016 *Science* **352** 1087

[93] Baur M, Filipp S, Bianchetti R, Fink J M, Göppl M, Steffen L, Leek P J, Blais A and Wallraff A 2009 *Phys. Rev. Lett.* **102** 243602

[94] Sillanpää M A, Li J, Cicak K, Altomare F, Park J I, Simmonds R W, Paraoanu G S and Hakonen P J 2009 *Phys. Rev. Lett.* **103** 193601

[95] Li J, Paraoanu G S, Cicak K, Altomare F, Park J I, Simmonds R W, Sillanpää M A and Hakonen P J 2011 *Phys. Rev. B* **84** 104527

[96] Novikov S, Robinson J E, Keane Z K, Suri B, Wellstood F C and Palmer B S 2013 *Phys. Rev. B* **88** 060503

[97] Suri B, Keane Z K, Ruskov R, Bishop L S, Tahan C, Novikov S, Robinson J E, Wellstood F C and Palmer B S 2013 *New J. Phys.* **15** 125007

[98] Kumar K S, Vepsäläinen A, Danilin S and Paraoanu G S 2016 *Nat. Commun.* **7** 10628

[99] Xu H K, Song C, Liu W Y, Xue G M, Su F F, Deng H, Tian Ye, Zheng D N, Han S, Zhong Y P, Wang H, Liu Y X and Zhao S P 2016 *Nat. Commun.* **7** 11018

[100] Novikov S, Sweeney T, Robinson J E, Premaratne S P, Suri B, Wellstood F C and Palmer B S 2016 *Nat. Phys.* **12** 75

[101] Liu Q C, Li T F, Luo X Q, Zhao H, Xiong W, Zhang Y S, Chen Z, Liu J S, Chen W, Nori F, Tsai J S and You J Q 2016 *Phys. Rev. A* **93** 053838

[102] Astafiev O, Zagoskin A M, Abdumalikov A A Jr, Pashkin Y A, Yamamoto T, Inomata K, Nakamura Y and Tsai J S 2010 *Science* **327** 840

[103] Peng Z H, Liu Y X, Peltonen J T, Yamamoto T, Tsai J S and Astafiev O 2015 *Phys. Rev. Lett.* **115** 223603

[104] Kadowaki T and Nishimori H 1998 *Phys. Rev. E* **58** 5355

[105] Brooke J, Bitko D, Rosenbaum T F and Aeppli G 1999 *Science* **284** 779

[106] Farhi E, Goldstone J, Gutmann S, Lapan J, Lundgren A and Preda D 2001 *Science* **292** 472

[107] Das A and Chakrabarti B K 2008 *Rev. Mod. Phys.* **80** 1061

[108] Aharonov D, van Dam W, Kempe J, Landau Z, Lloyd S and Regev O 2007 *SIAM J. Comput.* **37** 166

[109] Mizel A, Lidar D A and Mitchell M 2007 *Phys. Rev. Lett.* **99** 070502

[110] Harris R, Johnson M W, Lanting T, Berkley A J, Johansson J, Bunyk P, Tolkacheva E, Ladizinsky E, Ladizinsky N, Oh T, Cioata F, Perminov I, Spear P, Enderud C, Rich C, Uchaikin S, Thom M C, Chapple E M, Wang J, Wilson B, Amin M H S, Dickson N, Karimi K, Macready B, Truncik C J S and Rose G 2010 *Phys. Rev. B* **82** 024511

[111] Johnson M W, Amin M H S, Gildert S, Lanting T, Hamze F, Dickson N, Harris R, Berkley A J, Johansson J, Bunyk P, Chapple E M, Enderud C, Hilton J P, Karimi K, Ladizinsky E, Ladizinsky N, Oh T, Perminov I, Rich C, Thom M C, Tolkacheva E, Truncik C J S, Uchaikin S, Wang J, Wilson B and Rose G 2011 *Nature* **473** 194

[112] Harris R, Berkley A J, Johnson M W, Bunyk P, Govorkov S, Thom M C, Uchaikin S, Wilson A B, Chung J, Holtham E, Biamonte J D, Smirnov A Yu, Amin M H S and van den Brink A M 2007 *Phys. Rev. Lett.* **98** 177001

[113] Harris R, Johansson J, Berkley A J, Johnson M W, Lanting T, Han S, Bunyk P, Ladizinsky E, Oh T, Perminov I, Tolkacheva E, Uchaikin S, Chapple E M, Enderud C, Rich C, Thom M, Wang J, Wilson B and Rose G 2010 *Phys. Rev. B* **81** 134510

[114] Lanting T, Przybysz A J, Smirnov A Yu, Spedalieri F M, Amin M H, Berkley A J, Harris R, Altomare F, Boixo S, Bunyk P, Dickson N, Enderud C, Hilton J P, Hoskinson E, Johnson M W, Ladizinsky E, Ladizinsky N, Neufeld R, Oh T, Perminov I, Rich C, Thom M C, Tolkacheva E, Uchaikin S, Wilson A B and Rose G 2014 *Phys. Rev. X* **4** 021041

[115] Boixo S, Smelyanskiy V N, Shabani A, Isakov S V, Dykman M, Denchev V S, Amin M H, Smirnov A Yu, Mohseni M and H. Neven 2016 *Nat. Commun.* **7** 10327

[116] Denchev V S, Boixo S, Isakov S V, Ding N, Babbush R, Smelyanskiy V, Martinis J and Neven H 2016 *Phys. Rev. X* **6** 031015

[117] Smelyanskiy V N, Venturelli D, Perdomo-Ortiz A, Knysh S and Dykman M I 2017 *Phys. Rev. Lett.* **118** 066802

[118] Feynman R 1982 *Int. J. Theor. Phys.* **21** 467

[119] Cirac J I and Zoller P 2012 *Nat. Phys.* **8** 264

[120] Lloyd S 1996 *Science* **273** 1073

[121] Houck A A, Türeci H E and Koch J 2012 *Nat. Phys.* **8** 292

[122] Paraoanu G S 2014 *J. Low Temp. Phys.* **175** 633

[123] Las Heras U, Mezzacapo A, Lamata L, Filipp S, Wallraff A and Solano E 2014 *Phys. Rev. Lett.* **112** 200501

[124] Las Heras U, García-Álvarez L, Mezzacapo A, Solano E and Lamata L 2015 *EPJ Quantum Technol.* **2** 8

[125] Salath Y, Mondal M, Oppliger M, Heinsoo J, Kurpiers P, Potočnik A, Mezzacapo A, Las Heras U, Lamata L, Solano E, Filipp S and Wallraff A 2015 *Phys. Rev. X* **5** 021027

[126] Barends R, Lamata L, Kelly J, García-Álvarez L, Fowler A G, Megrant A, Jeffrey E, White T C, Sank D, Mutus J Y, Campbell B, Chen Yu, Chen Z, Chiaro B, Dunsworth A, Hoi I C, Neill C, O'Malley P J J, Quintana C, Roushan P, Vainsencher A, Wenner J, Solano E and Martinis J M 2015 *Nat. Commun.* **6** 7654

[127] Dallaire-Demers P L and Wilhelm F K 2016 *Phys. Rev. A* **94** 062304

[128] Dallaire-Demers P L and Wilhelm F K 2016 *Phys. Rev. A* **93** 032303

[129] Reiner J M, Marthaler M, Braumüller J, Weides M and Schön G 2016 *Phys. Rev. A* **94** 032338

[130] Zhong Y P, Xu D, Wang P, Song C, Guo Q J, Liu W X, Xu K, Xia B X, Lu C Y, Han S, Pan J W and Wang H 2016 *Phys. Rev. Lett.* **117** 110501

[131] Viehmann O, von Delft J and Marquardt F 2013 *Phys. Rev. Lett.* **110** 030601

[132] Kurcz A, Bermudez A and García-Ripoll J J 2014 *Phys. Rev. Lett.* **112** 180405

[133] Dalmonte M, Mirzaei S I, Muppalla P R, Marcos D, Zoller P and Kirchmair G 2015 *Phys. Rev. B* **92** 174507

[134] Mei F, Stojanović V M, Siddiqi I and Tian L 2013 *Phys. Rev. B* **88** 224502

[135] Stojanović V M, Vanević M, Demler E and Tian L 2014 *Phys. Rev. B* **89** 144508

[136] Seo K and Tian L 2015 *Phys. Rev. B* **91** 195439

[137] Seo K and Tian L 2015 *Sci. China-Phys. Mech. Astron.* **58** 070302

[138] Wang Z, Gu X, Wu L A and Liu Y X 2016 *Phys. Rev. A* **93** 062301

[139] You J Q, Shi X F, Hu X D and Nori F 2010 *Phys. Rev. B* **81** 014505

[140] Tanamoto T, Ono K, Liu Y X and Nori F 2015 *Sci. Rep.* **5** 10076

[141] DiVincenzo D P 2000 *Fortschr. Phys.* **48** 771

[142] Kelly J, Barends R, Fowler A G, Megrant A, Jeffrey E, White T C, Sank D, Mutus J Y, Campbell1 B, Chen Yu, Chen Z, Chiaro B, Dunsworth A, Hoi I C, Neill C, O'Malley P J J, Quintana C, Roushan P, Vainsencher A, Wenner J, Cleland A N and Martinis J M 2015 *Nature* **519** 66

[143] Ofek N, Petrenko A, Heeres R, Reinhold P, Leghtas Z, Vlastakis B, Liu Y, Frunzio L, Girvin S M, Jiang L, Mirrahimi M, Devoret M H and Schoelkopf R J 2016 *Nature* **536** 441

[144] Barends R, Kelly J, Megrant A, Veitia A, Sank D, Jeffrey E, White T C, Mutus J, Fowler A G, Campbell B, Chen Y, Chen Z, Chiaro B, Dunsworth A, Neill C, O'Malley P, Roushan P, Vainsencher A, Wenner J, Korotkov A N, Cleland A N and Martinis J M 2014 *Nature* **508** 500

[145] Song C, Xu K, Liu W, Yang C, Zheng S B, Deng H, Xie Q, Huang K, Guo Q, Zhang L, Zhang P, Xu D, Zheng D, Zhu X, Wang H, Chen Y A, Lu C Y, Han S and Pan J W 2017 arXiv: 1703.10302

[146] DiCarlo L, Chow J M, Gambetta J M, Bishop L S, Johnson B R, Schuster D I, Majer J, Blais A, Frunzio L, Girvin S M and Schoelkopf R J 2009 *Nature* **460** 240

[147] Zheng Y, Song C, Chen M C, Xia B, Liu W, Guo Q, Zhang L, Xu D, Deng H, Huang K, Wu Y, Yan Z, Zheng D, Lu Li, Pan J W, Wang H, Lu C Y and Zhu X 2017 *Phys. Rev. Lett.* **118** 210504

[148] Risté D, da Silva M P, Ryan C A, Cross A W, Córcoles A D, Smolin J A, Gambetta J M, Chow J M and Johnson B R 2017 *NPJ Quantum Information* **3** 16

[149] Liu Q, Li M M, Dai K Z, Zhang K, Xue G M, Tan X S, Yu H F and Yu Y 2017 *Appl. Phys. Lett.* **110** 232602

[150] Versluis R, Poletto S, Khammassi N, Haider N, Michalak D J, Bruno A, Bertels K and DiCarlo L 2016 arXiv: 1612.08208

[151] Rosenberg D, Kim D, Das R, Yost D, Gustavsson S, Hover D, Krantz P, Melville A, Racz L, Samach G O, Weber S J, Yan F, Yoder J, Kerman A J and Oliver W D 2017 arXiv: 1706.04116